

Quantum Divide and Conquer for Classical Shadows

Daniel T. Chen¹, Zain H. Saleem¹, and Michael A. Perlin²

¹Mathematics and Computer Science Division, Argonne National Laboratory

²Super.tech division of Inflexion, 5235 S Harper Ct, Chicago, IL 60615

Classical shadow tomography is a sample-efficient technique for characterizing quantum systems and predicting many of their properties. Circuit cutting is a technique for dividing large quantum circuits into smaller fragments that can be executed more robustly using fewer quantum resources. We introduce a divide-and-conquer circuit cutting method for estimating the expectation values of observables using classical shadows. We derive a general formula for making predictions using the classical shadows of circuit fragments from arbitrarily cut circuits. In addition, we provide the sample complexity required to estimate an observable to a desired additive error with high probability. Lastly, we numerically show that our divide-and-conquer method outperforms traditional uncut shadow tomography when estimating high-weight observables that act nontrivially on many qubits, and discuss the mechanisms for this advantage.

1 Introduction

The complexity of fully describing a quantum system grows exponentially with its size. However, it may be considerably easier to estimate certain properties of a quantum state. To leverage this idea, Aaronson introduced the concept of *shadow tomography* [1]. Aaronson proved that some functions of a quantum state, namely expectation values of a fixed but arbitrary set of observables, can be estimated arbitrarily well using only polynomially many copies of the quantum state. However, Aaronson’s procedure required capabilities that are well out of reach for near-term experiments and quantum computing devices. Inspired by the idea of estimating properties rather than states themselves, Huang, Kueng, and Preskill recast Aaronson’s method into *classical shadow tomography*, which retains the original method’s favorable complexity while alleviating hardware constraints [2–4]. On a high level, Huang *et al.*’s shadow tomography builds a classical model of a quantum state, or a *classical shadow*, that can be used to estimate the desired observables.

Classical shadow tomography, including its randomized [2–4], derandomized [5, 6], and Bayesian [7] variants, has subsequently received a great deal of attention. Classical shadows have been shown to be beneficial for machine learning [8, 9], avoiding barren plateaus [10], estimating fermionic states [11], and mitigating errors [12]. Classical shadows are also provably robust to various types of noise [8, 13], which demonstrates compatibility with noisy near-term quantum computing devices. The channel-state duality also allows the techniques of classical shadows to be used for efficient quantum process tomography [14, 15].

Meanwhile, inspired by fragmentation methods for molecular simulation [16–19], Peng *et al.* recently introduced the idea of *circuit cutting* [20]. Circuit cutting divides a large

quantum circuit into smaller subcircuits, or *fragments*. These fragments can be simulated independently and subsequently recombined by classically post-processing their measurement results. Circuit cutting can thereby reduce the number of qubits required to simulate a quantum circuit. This technique is also sometimes referred to as *circuit knitting*.

Generally speaking, circuit cutting comes at the cost of classical post-processing overheads that are exponential in the number of cuts that are made to a circuit. However, these overheads might be avoided with suitably-designed algorithms that use circuit cutting for distributed quantum combinatorial optimization [21]. Moreover, recent studies have demonstrated that circuit cutting allows quantum circuits to be more reliably executed, and that circuit cutting can be beneficial even if a quantum device has enough qubits to simulate the entire circuit [22–24]. More elaborate circuit cutting procedures have also been proposed. For example, maximum likelihood methods have been applied to mitigate the corrupting effect of hardware errors and shot noise on recombined circuit outputs [24]. Circuit cutting can also be sped up by incorporating randomized measurements [25] or stochastic classical postprocessing [26]. Other work has proposed to fragment a circuit by cutting gates rather than wires [27].

In this work, we introduce a divide-and-conquer circuit cutting method for estimating the expectation values of observables from the classical shadows of circuit fragments. With the circuit-cutting formalism, we express the expectation values at the end of a circuit in terms of the classical shadows of its fragments. This formalism inherits the flexibility and low sample complexity of classical shadows, while allowing for the simulation of smaller quantum circuits. We further show that circuit cutting enables estimating higher-weight observables (that is, observables that act non-trivially on more qubits) with a fixed number of measurement samples. In total, we find that if a quantum circuit is amenable to cutting, doing so increases the weight of the observables that can be accurately estimated using classical shadow tomography.

The organization of the paper is as follows. We review circuit cutting in Section 2, and derive a general formula for using fragment data to estimate expectation values with respect to the output state of a fragmented circuit. In Section 3, we review shadow tomography, a derandomized variant thereof, and the use of classical shadows for quantum process tomography. Section 4 combines circuit cutting and shadow tomography, providing theoretical lower bounds on the sample complexity of estimating observables using the classical shadows of fragments, as well as numerical results comparing shadow tomography with and without fragmentation.

1.1 Notational Remarks

Since the paper will be concerned with quantum circuits, we will uniformly index each qubit wire starting from 1. Numerical subscripts will be reserved for actions on qubits specified by an index. For example, U_{12} will be a quantum gate U acting on qubits 1 and 2. Similarly, we will use numerical indices to denote partial traces, such that $\text{tr}_1(\rho)$ denotes the partial trace of ρ with respect to qubit 1.

For an operator A , A^\top will be used to denote the matrix transpose and A^\dagger will be used to denote its adjoint operator (conjugate transpose). Sets are usually denoted with script-characters like \mathcal{S} or greek letters. Complements will be denoted by $\overline{\mathcal{S}}$. However, if set complements ever occurs in subscripts, slashes will be used for cleaner typesetting, *e.g.* $A_{\mathcal{S}}$. Moreover, for a positive integer N , the set $[N]$ is the set that enumerates from 1 to N , *i.e.* $[N] = \{1, 2, \dots, N\}$.

2 Quantum circuit cutting

Consider three-qubit quantum state prepared by a circuit $\rho = V_{23}U_{12}|000\rangle\langle 000|U_{12}^\dagger V_{23}^\dagger$ for some arbitrary two-qubit quantum gates U_{12} and V_{23} . Let \mathcal{B} be an orthogonal basis for the vector space of 2×2 matrices, such that $\text{tr}(AB) = 2$ if $A = B$ and 0 otherwise for all $A, B \in \mathcal{B}$. In the rest of the paper, we will use the Pauli matrices for concreteness, $\mathcal{B} = \{I, X, Y, Z\}$. The orthogonality of \mathcal{B} with respect to the trace inner product implies that ρ can be expanded into a sum of tensor products as

$$\rho = \frac{1}{2} \sum_{M \in \mathcal{B}} \text{tr}_2 \left(M_2 U_{12} |00\rangle\langle 00| U_{12}^\dagger \right) \otimes V_{23} (M_2 \otimes |0\rangle\langle 0|) V_{23}^\dagger, \quad (1)$$

where M_2 denotes the action of M on qubit 2. The two tensor factors inside the summation essentially form two quantum states (clarified below) that can be prepared independently. Thus, we say that the quantum circuit can be *cut* into two *fragments*, f_1 and f_2 . The state of each fragment is parameterized by the operator $M \in \mathcal{B}$, satisfying:

$$\rho_{f_1}(M) = \text{tr}_2 \left(M_2 U_{12} |00\rangle\langle 00| U_{12}^\dagger \right), \quad (2)$$

$$\rho_{f_2}(M) = V_{23} (M_2 \otimes |0\rangle\langle 0|) V_{23}^\dagger. \quad (3)$$

Careful readers should note that $\rho_{f_i}(M)$ is not actually a “state” since M is a (possibly traceless) operator rather than a quantum state. To resolve this concern, we interpret ρ_{f_j} as a linear combination of *conditional states* by expanding $M = rM^{(r)} + sM^{(s)}$, where $(r, s) = \lambda(M)$ are the eigenvalues of M , and $M^{(j)}$ is a rank-1 projector. Then, we complete the conditional-state interpretation of Eq. (1) with the expansion

$$\rho = \frac{1}{2} \sum_{\substack{M \in \mathcal{B}, \\ r, s \in \lambda(M)}} rs \cdot \rho_{f_1}(M^{(r)}) \otimes \rho_{f_2}(M^{(s)}). \quad (4)$$

In the following text, we will not make the distinction between Eqs. (1) and (4) for notational cleanliness.

One can think of circuit cutting as performing tomography at the cut locations. We will call the qubit wire directly upstream of the cut a *quantum output*, which is connected to a *quantum input* directly downstream of the cut. Circuit cutting is performed by inferring all quantum degrees of freedom at the cut locations—summing over an informational-complete (IC) set of measurement bases at quantum outputs, and over IC set of states (such as the SIC-POVM states [28]) at quantum inputs. On the other hand, the *circuit output* of a fragment are the qubit wires that were at the end of the uncut circuit. The ultimate goal is to combine data collected from fragments in a way that reproduces desired properties of the full, uncut circuit.

In this paper, we focus on reconstructing the expectation value of an observable O with respect to the state ρ prepared by a circuit, *i.e.* $\text{tr}(O\rho)$. For concreteness, suppose O admits the decomposition $O = O_1 \otimes O_{23}$, and that the circuit preparing ρ is amenable to cutting as in Eq. (1). Then, we can write the expectation value as a sum of products of expectations with respect to operators that are local to each fragment:

$$\text{tr}(O\rho) = \frac{1}{2} \sum_{M \in \mathcal{B}} \text{tr} [(O_1 \otimes O_{23}) \cdot (\rho_{f_1}(M) \otimes \rho_{f_2}(M))] \quad (5)$$

$$= \frac{1}{2} \sum_M \text{tr}[O_1 \rho_{f_1}(M)] \cdot \text{tr}[O_{23} \rho_{f_2}(M)]. \quad (6)$$

We can reformulate the above equation in a way that abandons the distinction between initialization and measurements. Each fragment can be viewed as a quantum channel that maps a state at the quantum input of a fragment to a state at all outputs (including both quantum outputs that are associated with a cut, and circuit outputs that are not). By the channel-state duality [29–31], we can write the quantum channel as a tripartite *Choi state*, denoted by Λ , and the expectation can be written as the following.

$$\text{tr}(O\rho) = \sum_M \text{tr}((M \otimes O_1)\Lambda_{f_1}) \cdot \text{tr}((M^\top \otimes O_{23})\Lambda_{f_2}) \quad (7)$$

Note the distinction between a *Choi matrix* and a Choi state. Here, we invoke the state interpretation, which requires a normalization factor that scales with the dimension of the quantum input. Thus, the factor of $1/2$ that we see in Eq. (6) is absorbed into Λ_{f_2} . No normalization is needed for Λ_{f_1} because it lacks quantum inputs.

2.1 Generalizing circuit cutting

A circuit can be cut at arbitrary locations so long as it forms distinct fragments that can be operated on. Tang *et al.* proposed methods for optimizing the cut location based on post-processing complexity [32]. We will consider the case where the cut locations have already been decided. Fragments and their connectivity can then be represented by a directed graph with fragments as vertices and qubit wires connecting fragments as edges.

More formally, an N_q -qubit quantum circuit is split up into fragments $F = \{f_i\}_{i=1}^{N_f}$ with K cuts. The collection of fragments forms a directed multigraph $G = (F, E)$ where each edge $(f_i, f_j, \ell) \in E$ represents a cut on qubit ℓ separating fragment f_i from fragment f_j . Furthermore, let $\mathcal{P}(f_j)$ be the set of fragments that are “upstream” of f_j in G , *i.e.* the set of fragments f_i for which there exists a path in G from f_i to f_j . For each fragment f_i , there is an associated quantum state ρ_{f_i} (of its circuit outputs) that depends on some auxiliary operators $M \in \mathcal{B}$, which in turn dictate state preparation (quantum input) and measurement (quantum output) routines. Lastly, $\mathcal{Q}_i(f_i), \mathcal{Q}_o(f_i), \mathcal{C}_o(f_i)$ denote the number of quantum inputs, quantum outputs, and circuit outputs associated with fragment f_i .

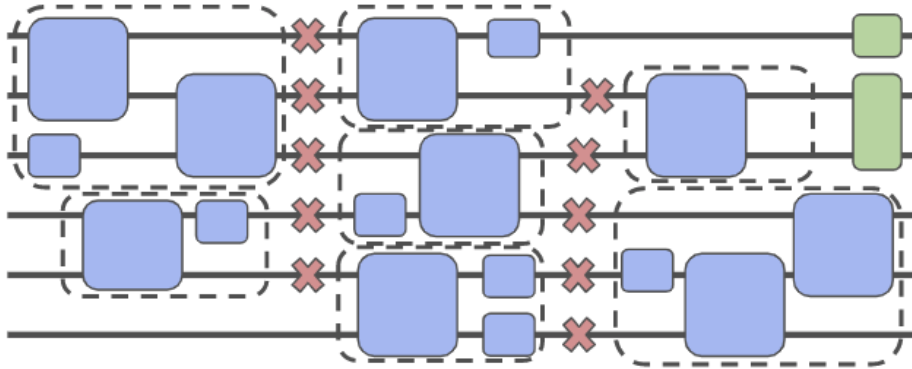
Given an arbitrary circuit split into N_f fragments $\{f_i\}$ with K cuts, the quantum state prepared by the circuit can be written (up to a permutation of qubits) as

$$\rho = \frac{1}{2^K} \sum_{M \in \mathcal{B}^K} \bigotimes_{i=1}^{N_f} \rho_{f_i}(M_{f_i}), \quad (8)$$

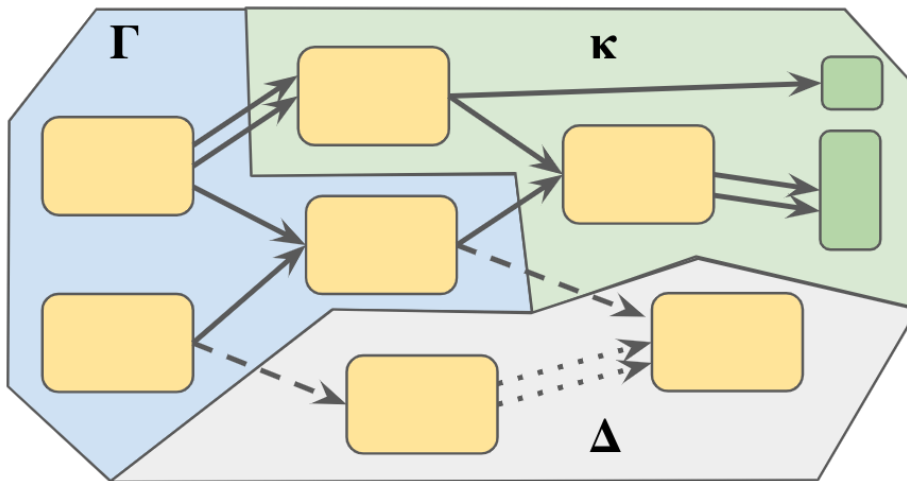
where M_{f_i} denotes the operators in M that are associated with the cuts incident to fragment f_i . So, M_{f_i} is a tuple of $\mathcal{Q}_i(f_i) + \mathcal{Q}_o(f_i)$ operators in \mathcal{B} . It is also important to note that we will allow fragments with no circuit outputs, in which case $\rho_{f_i}(M_{f_i})$ is simply a scalar.

Consider an operator O that is local to a subset $\mathcal{K} \subset [N_q]$ of the qubits that are addressed by a circuit. Let κ be the set of fragments that have circuit outputs on the qubits in \mathcal{K} . Furthermore, let $O^{(\kappa)}$ be the restriction of O onto the circuit outputs of fragments in κ ; by definition, O acts trivially on all other fragments. We can separate expectation values of O into factors involving the fragments that are addressed by O , namely κ , and all other fragments, $\bar{\kappa} = F \setminus \kappa$:

$$\text{tr}(O\rho) = \frac{1}{2^K} \sum_{M \in \mathcal{B}^K} \text{tr} \left(O^{(\kappa)} \bigotimes_{f_k \in \kappa} \rho_{f_k}(M_{f_k}) \right) \cdot \prod_{f_i \in \bar{\kappa}} \text{tr}(\rho_{f_i}(M_{f_i})). \quad (9)$$



(a) Above is an example of circuit cutting. Blue boxes represent arbitrary quantum gates, red crosses represent cut locations, and dashed lines outline individual fragments. The two green boxes at the end of the circuit represent observables that we wish to find the expectation of.



(b) Given the circuit and cut on the left, we can construct a fragment graph as depicted above. Each yellow box corresponds to one fragment. Each shaded region represents one part in the fragment graph partition. The green region (κ) denotes the fragments directly acted on by the observable. The blue region (Γ) denotes the fragment that are upstream of κ . The grey region denotes the fragments in Δ , which does not contribute to the expectation value of the desired observable.

Figure 1: An example of circuit cutting and its mapping to a fragment graph.

It is important to note that these expressions assume that tensor factors are permuted to the appropriate ordering, which will be an implicit assumption throughout this work.

We now seek to eliminate the dependence of $\text{tr}(O\rho)$ on fragments that are outside the past light cone of O . To this end, we further partition the set $\bar{\kappa}$, as visualized in Figure 1. Let $\Gamma = \bigcup_{k \in \kappa} \mathcal{P}(f_k) \cap \bar{\kappa}$ be the set of fragments upstream of κ in G , and let $\Delta = F \setminus (\kappa \cup \Gamma)$ be the set of all remaining fragments in G . In terms of this decomposition, we have

$$\text{tr}(O\rho) = \frac{1}{2^K} \sum_{M \in \mathcal{B}^K} \text{tr} \left(O^{(\kappa)} \bigotimes_{f_k \in \kappa} \rho_{f_k}(M_{f_k}) \right) \cdot \prod_{f_i \in \Gamma} \text{tr}(\rho_{f_i}(M_{f_i})) \cdot \prod_{f_j \in \Delta} \text{tr}(\rho_{f_j}(M_{f_j})). \quad (10)$$

Partition of the edge set E of G into three parts: (a) the edges E_Δ in Δ , (b) the edges $E_{\bar{\Delta}}$ in the complement $\bar{\Delta} = \kappa \cup \Gamma$, and (c) the edges $E_{\bar{\Delta} \rightarrow \Delta}$ from $\bar{\Delta}$ to Δ . We can sum over all operators in Eq. (10) that are associated with edges in E_Δ to contract all fragments in Δ into a single fragment f_Δ :

$$\text{tr}(O\rho) = \frac{1}{2^{K-|E_\Delta|}} \sum_{M \in \mathcal{B}^{K-|E_\Delta|}} \text{tr} \left(O^{(\kappa)} \bigotimes_{f_k \in \kappa} \rho_{f_k}(M_{f_k}) \right) \cdot \prod_{f_i \in \Gamma} \text{tr}(\rho_{f_i}(M_{f_i})) \cdot \text{tr}(\rho_{f_\Delta}(M_{f_\Delta})). \quad (11)$$

Here M_{f_Δ} contains only operators associated with the edges $E_{\bar{\Delta} \rightarrow \Delta}$. Viewing ρ_{f_Δ} as a trace-preserving quantum channel from its quantum inputs to its circuit outputs, we observe that $\text{tr}(\rho_{f_\Delta}(M_{f_\Delta})) = 0$ unless all operators in M_{f_Δ} have nonvanishing trace, which only occurs if they are all the identity operator, in which case $\text{tr}(\rho_{f_\Delta}(M_{f_\Delta})) = 2^{|E_{\bar{\Delta} \rightarrow \Delta}|}$. Altogether,

$$\text{tr}(O\rho) = \frac{1}{2^{|E_\Delta|}} \sum_{M \in \mathcal{B}^{|E_\Delta|}} \text{tr} \left(O^{(\kappa)} \bigotimes_{f_k \in \kappa} \rho_{f_k}(M_{f_k}) \right) \cdot \prod_{f_i \in \Gamma} \text{tr}(\rho_{f_i}(M_{f_i})), \quad (12)$$

where we used the fact that $K = |E_\Delta| + |E_{\bar{\Delta}}| + |E_{\bar{\Delta} \rightarrow \Delta}|$, and for brevity we implicitly assign identity operators to the quantum outputs of ρ_{f_k} and ρ_{f_i} that are associated with edges in $E_{\bar{\Delta} \rightarrow \Delta}$ (which is equivalent to simply tracing over these quantum outputs). Note that $\text{tr}(O\rho)$ is always independent of fragments in Δ .

The above expression assumes that the $O^{(\kappa)}$ can be measured directly, which may not always be the case. Expanding $O^{(\kappa)}$ in the basis of Pauli strings as $O^{(\kappa)} = \sum_{P \in \mathcal{B}^{\otimes |\kappa|}} \alpha_P P$, we find that

$$\text{tr}(O\rho) = \sum_{P \in \{I, X, Y, Z\}^{\otimes |\kappa|}} \frac{\alpha_P}{2^{|E_\Delta|}} \sum_{M \in \mathcal{B}^{|E_\Delta|}} \prod_{f_k \in \kappa} \text{tr} \left(P_{C_o(f_k)} \rho_{f_k}(M_{f_k}) \right) \cdot \prod_{f_i \in \Gamma} \text{tr}(\rho_{f_i}(M_{f_i})), \quad (13)$$

where $P_{C_o(f_k)}$ is the restriction of P to the circuit outputs of fragment f_k . The choice of Pauli-string expansion is for generality. Practically, the cost of obtaining the Pauli string expansion grows exponentially with respect to the size of O . One can employ alternative expansions so long as the decomposed observables are separable with respect to the circuit outputs of the fragments.

We can further apply the channel-state duality to each factor of the expansion in Eq. (13). Let $M_{f_i}^{Q_i}$ be a tensor product of operators at the quantum inputs of fragment f_i , and similarly $M_{f_i}^{Q_i^o}$ for the quantum outputs. Then, we can write the above summation

in terms of Choi states as

$$\begin{aligned} \text{tr}(O\rho) = & \sum_{P \in \{I, X, Y, Z\}^{\otimes |\kappa|}} \alpha_P \sum_{M \in \mathcal{B}^{|E_{\Delta}|}} \prod_{f_k \in \kappa} \text{tr} \left(\left(M_{f_k}^{Q_i^\top} \otimes M_{f_k}^{Q_o} \otimes P_{\mathcal{C}_o(f_k)} \right) \Lambda_{f_k} \right) \\ & \cdot \prod_{f_i \in \Gamma} \text{tr} \left(\left(M_{f_i}^{Q_i^\top} \otimes M_{f_i}^{Q_o} \otimes I_{\mathcal{C}_o(f_i)} \right) \Lambda_{f_i} \right), \end{aligned} \quad (14)$$

where $I_{\mathcal{C}_o(f_i)}$ is the identity operator on all circuit outputs of fragment f_i . As in Eq. (7), normalizing factors of 2 get absorbed into Choi states, since there are exactly $|E_{\Delta}|$ quantum inputs between the fragments in $\kappa \cup \Gamma$.

To summarize, we presented a general formula for finding the expectation of an observable in terms of expectations of operators on individual fragments. We can see that the formula sums over exponentially many terms with respect to the number of cuts. This is generally unavoidable without making further assumptions on a specific circuit ansatz. For an observable that is local to certain qubits, only the fragments that are directly acted on and the fragments upstream of those (that is, fragments in the past light cone of the observable) need to be considered. This decreases the exponential factor by a constant, which would correspond to an improvement in computational efficiency in practice.

3 Shadow tomography for states and processes

Quantum tomography refers reconstructing an unknown quantum state from measurements. The traditional method requires exponentially many measurements [33]. Though expensive, tomography is useful when the quantity to be estimated is not known a priori. *Classical shadow tomography* offers a computationally efficient way of estimating polynomially many observables with sub-exponential sample complexity [2]. Intuitively, shadow tomography aims at reconstructing properties of a quantum state by taking “snapshots” in random bases.

Formally, we shall begin by defining the *measurement primitive* \mathcal{U} —the set of measurement bases to sample from. The measurement primitive can be arbitrary so long as it is *tomographically complete*, *i.e.* for all quantum states $\sigma \neq \rho$, there exists a $U \in \mathcal{U}$ and $|b\rangle$ such that

$$\langle b|U\sigma U^\dagger|b\rangle \neq \langle b|U\rho U^\dagger|b\rangle \quad (15)$$

In this paper, we will employ the *random Pauli basis* measurement primitive:

$$\mathcal{U} = \{I, H, S^\dagger H\}^{\otimes n} = \text{Cl}(2)^{\otimes n} \quad (16)$$

where H is the Hadamard gate, $S = e^{-i\pi Z/4}$ is the S gate, which along with the identity forms the set of Clifford gates $\text{Cl}(2)$. Equivalently, one can think of this measurement primitive as measuring in a randomly-chosen Pauli basis. This measurement primitive has the property that the number of measurements needed to estimate expectation values of observables will scale exponentially only with the number of qubits that the observable acts on non-trivially, which we define as the size, or weight, of an observable O , and denote $\text{size}(O)$.

The general shadow tomography procedure, taken from [2], is as follows. After executing a circuit that prepares the state ρ , we pick $U \in \mathcal{U}$ uniformly at random, rotate $\rho \mapsto U\rho U^\dagger$, and measure all qubits in the computational basis. Suppose we get the measurement result $|b\rangle$. Then, we define a new operator \mathcal{M} by

$$\mathcal{M}(\rho) = \mathbb{E} \left(U^\dagger |b\rangle \langle b| U^\dagger \right) = \mathbb{E}_{U \sim \mathcal{U}} \sum_{b \in \{0,1\}^n} U^\dagger |b\rangle \langle b| U \langle b| U \rho U^\dagger |b\rangle. \quad (17)$$

From here, we build an estimator for ρ by inverting \mathcal{M} ,

$$\hat{\rho} = \mathcal{M}^{-1} \left(U^\dagger |\hat{b}\rangle \langle \hat{b}| U \right), \quad (18)$$

where the inverse of \mathcal{M} depends on the measurement primitive \mathcal{U} , and $\hat{\rho}$ is equal to ρ in expectation: $\mathbb{E}\hat{\rho} = \rho$. This inverse is well-defined because \mathcal{U} is tomographically complete. This estimator is the *classical shadow* of ρ , and generally speaking a classical shadow can be built by averaging over many such estimators. For more robust estimation, as suggested in Ref. [2], one could perform median-of-means—separating the shadow into groups of single-shot estimators, finding the mean estimate of each group, and taking the median of those means. Below we will give a theorem for the sample complexity of estimating linear functions.

Lemma 1 (Theorem 2 of Ref. [2]). *For the random Pauli measurement primitive \mathcal{U} , collection of Hermitian $O_1, \dots, O_M \in \mathbb{C}^{2^n \times 2^n}$, error $\epsilon, \delta \in (0, 1)$. Let*

$$K = 2 \log \frac{2M}{\delta}, \quad N = \frac{34}{\epsilon^2} \max_{i \in [M]} 4^{\text{size}(O_i)} \|O_i\|_\infty^2. \quad (19)$$

Then, a collection of NK independent classical shadows builds the estimator \hat{o}_i for the expectation of O_i satisfying

$$|\hat{o}_i - \text{tr}(O_i \rho)| < \epsilon \quad (20)$$

for all $i \in [M]$ with probability at least $1 - \delta$.

To obtain estimates of polynomially many observables, one would need only logarithmically growing numbers of measurements. Meanwhile, the number of measurements respects locality (which here means the number of qubits addressed by an operator, and has nothing to do with locality in physical space). For observables that are local to a few qubits, relatively few samples will be needed. Lastly, the choice of observables is not required a priori so long as there is an estimate for the maximum locality of observables.

3.1 Implementation of shadow tomography

Here we present an implementation that is equivalent to shadow tomography scheme above [5, 34]. Suppose we want to estimate the expectation of a Pauli observable O . The idea is to generate an ensemble of bitstrings measured in randomly chosen Pauli basis and collect only those that matches O at non-trivial qubits. The estimator is then generated by averaging over the bitstrings where O is directly observed.

Procedurally, for an n -qubit circuit we first generate an ensemble of length- n *trit-strings* s_1, s_2, \dots, s_S , where each $s_j \in \{X, Y, Z\}^n$ specifies a measurement basis for each qubit. For each trit-string s_j , we run the desired circuit and measure in basis specified by the string, obtaining a bitstring $m_j \in \{+1, -1\}^n$ that specifies the measurement outcome for each qubit. The collection of all trit-strings and corresponding measurement outcomes, $\{(s_j, m_j)\}_{j=1}^S$, is the classical shadow of the circuit. To estimate the expectation value of a Pauli observable O that acts non-trivially on qubits \mathcal{K} , we find a corresponding trit-string s_j that matches O at qubits \mathcal{K} , and take a product over the associated measurement outcomes in m_j at \mathcal{K} for a single-shot estimate of O . Lastly, we take an average of these single-shot estimates to get the final estimate for the expectation value of O .

For example, suppose there is a 3-qubit circuit. First, we generate the bases in which to measure each qubit in each independent evaluation of the circuit, and we get

$$(X, Y, X), (Z, Y, Y), (X, Z, Y), (X, Y, Z), (X, X, X). \quad (21)$$

Running the circuit yields an ensemble of bitstrings like the following:

$$(1, 1, -1), (-1, -1, 1), (-1, 1, -1), (-1, 1, 1), (1, -1, 1). \quad (22)$$

Suppose we want to estimate the expectation value of $O = XYI$. We then look for occurrences of (X, Y, \cdot) —corresponding to XYI —and collect only the parts of the classical shadow that matches this pattern. We end up with bitstrings $(1, 1, -1)$ and $(-1, 1, 1)$. Again, only the measurement outcome of the first two qubits matter, so we get a final estimate of $((1 \times 1) + (-1 \times 1))/2 = 0$. On the other hand, if $O = IYI$, then our estimate becomes $(1 - 1 + 1)/3 = 1/3$. Of course, there is a chance that the corresponding Pauli string is simply not observed, *e.g.* if $O = YXI$. In this case, there is simply no data that allows us to return an informed estimate and, as a default, we return the uniform prior on O , namely $\text{tr}(O) = 0$ (for nontrivial Pauli observables). As we will see in Section 4.2, this phenomenon is a significant drawback of shadow tomography, which can be greatly mitigated with circuit fragmentation.

3.2 Shadow process tomography

Process tomography refers to inferring a quantum channel, a completely-positive map between Hilbert spaces, from measurements. For a fixed number of qubits, process tomography is in general exponentially more expensive than state tomography because we are required to map each input—a quantum state—to its output—another quantum state. By the channel-state duality, the problem of process tomography can be reduced to performing state tomography on the Choi state, from which we can directly apply the results from shadow tomography [14, 15].

Suppose we wish to know about a quantum channel \mathcal{E} with Choi state $\Lambda \in \mathbb{C}^{2^{m+n} \times 2^{m+n}}$. Suppose ρ is the input state and σ is the output state, then by channel-state duality, the probability of the mapping $\rho \mapsto \sigma$ occurring can be thought of as performing a measurement on the Choi state.

$$\Pr(\mathcal{E}(\rho) \mapsto \sigma) = \text{tr}((\rho^\top \otimes \sigma)\Lambda) \quad (23)$$

Define the operator $O = \rho^\top \otimes \sigma$. Like in shadow tomography, we can have a collection of operators O , *i.e.* O_1, O_2, \dots, O_M each specifying an input-output relation we wish to predict.

Just like in shadow state tomography, we pick a measurement primitive \mathcal{U} . Then, there are two equivalent ways of obtaining the classical shadow, as depicted in Figure 2. The first method straightforwardly applies random unitaries on both the input (immediately before the channel) and output prior to measuring the outcome. Equivalently, one can accomplish the same task by having the same number of ancilla qubits prepared as the dimension of the input, maximally entangle the ancilla and input qubits, and apply the random unitary altogether to the $n + m$ qubits (output + ancilla) at the end prior to measurement. Our numerical implementation uses the latter strategy, and measuring gives bitstrings $\hat{b} \in \{0, 1\}^{n+m}$ that can be used to build the shadow of the Choi matrix.

$$\hat{\Lambda} = \mathcal{M}^{-1} \left(U^\dagger |\hat{b}\rangle \langle \hat{b}| U \right) \quad (24)$$

All procedures and results from state tomography are now transferable to process tomography. That is, to query polynomially many input-output relationships, the sample complexity scales only logarithmically with the number of these relationships. As each fragment can be viewed as a quantum channel from its quantum inputs to all of its outputs, the capability of building classical shadows of quantum channels becomes crucial for obtaining classical shadows of fragmented circuits.

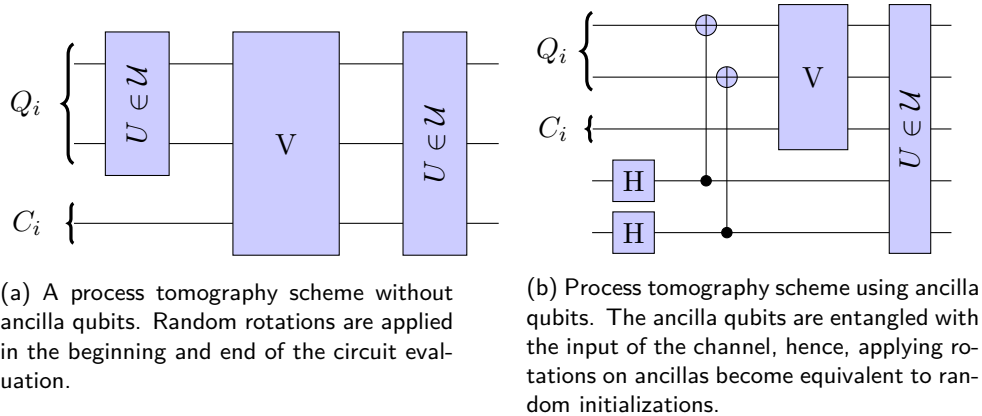


Figure 2: Two equivalent circuits for shadow process tomography of an arbitrary quantum channel V . Unitaries picked from a measurement primitive \mathcal{U} can be **(left)** applied both the quantum inputs and outputs directly, or **(right)** applied at the end of the circuit using ancillas.

4 Classical shadows of fragmented circuits

A divide and conquer algorithm for classical shadow tomography follows directly from combining the results of the two previous sections. Eq. (14) writes the expectation of an observable O with respect to a circuit-induced state ρ as sums and products of expectations with respect to Choi states of necessary fragments. Thus, to obtain classical shadows of a fragmented circuit, one simply sample shadows from the Choi state via the channel-state duality and shadow process tomography. Like any circuit-cutting procedure, shadow tomography can be performed independently on each fragment in a distributed manner. Moreover, this method does not assume the observable of interest, O , a priori. Having classical shadows of all fragments is equivalent to having classical shadows of the uncut state prepared by a circuit, and subsequent circuit reductions as instructed in Eq. (12) can be performed once an observable O is chosen. Lastly, classical shadows of fragments can be reused when multiple observables, O_1, O_2, \dots, O_M , are of interest. As in the case of ordinary shadow tomography, the number of measurements needed grows logarithmically with M .

4.1 Sample complexity of divide and conquer

Once the shadows of fragments are obtained, it is preferable to have theoretical guarantees that once operations in Eq. (14) are performed, the final estimate of $\text{tr}(O\rho)$ is close to the true value. Below, we present the sample complexity of each fragment for estimating the expectation of a single observable O . For each fragment, the same ensemble of classical shadows will be used to obtain information about the quantum input and output in addition to the circuit output if present. As a result, the sample complexity of each fragment is highly dependent on the degree of the fragment on the corresponding multigraph. The formal statement is provided below.

Theorem 1. *Consider a quantum state ρ from a circuit that is cut into fragments with the corresponding fragment graph $G = (F, E)$ and a $|\mathcal{K}|$ -local observable O . Define the degree of a fragment be the sum of its number of quantum input, quantum output, and circuit output.*

$$\text{deg}(f_k) = Q_i(f_k) + Q_o(f_k) + C_o(f_k), \quad \text{qdeg}(f_k) = Q_i(f_k) + Q_o(f_k) \quad (25)$$

Then, for any $\epsilon, \delta \in (0, 1)$ and a fixed fragment f_k , let

$$K_{f_k} = 2^{\text{qdeg}(f_k)+1} \log \frac{2|F|}{\delta}, \quad N_{f_k} = \frac{34(|\kappa| + |\Gamma|)}{\epsilon^2} 4^{\text{deg}(f_k)+2|E_{\Delta}|} \|O\|_S^4 \quad (26)$$

where $\|\cdot\|_S$ is the Pauli-string norm (c.f. Equation 38). Then, a collection of $N_{f_k} \cdot K_{f_k}$ independent classical shadows for each fragment $f_k \in F$ can estimate $\text{tr}(O\rho)$ with (expected) additive error ϵ with probability at least $1 - \delta$ (neglecting higher order terms).

The theorem above gives the ‘‘per-fragment’’ sample complexity for estimating the expectation of an observable with respect to an uncut circuit. The analysis requires simple facts regarding propagation of error when taking sums and products of perturbed quantities. These tools are proved as lemmas below.

Lemma 2. Let $(\hat{a}_i)_{i=1}^n$ be a collection of independent random variables satisfying $\mathbb{E}(\hat{a}_i - a_i) = 0$, $|a_i| \leq 1$, and $\mathbb{E}(\hat{a}_i - a_i)^2 = \epsilon^2$. Then,

$$\text{std} \left(\prod_i \hat{a}_i - \prod_i a_i \right) = \sqrt{n}\epsilon + \mathcal{O}(\epsilon^2). \quad (27)$$

Proof. We start with the first statement. Consider the case of $n = 2$. Using the independence of a_i ’s, we get that

$$\mathbb{E}(\hat{a}_1 \hat{a}_2 - a_1 a_2)^2 = \mathbb{E}(\hat{a}_1^2 \hat{a}_2^2) - 2a_1 a_2 \mathbb{E}(\hat{a}_1 \hat{a}_2) + a_1^2 a_2^2 = \mathbb{E} \hat{a}_1^2 \mathbb{E} \hat{a}_2^2 - a_1^2 a_2^2, \quad (28)$$

where we can substitute $\mathbb{E} \hat{a}_i^2 = \mathbb{E}(\hat{a}_i - a_i)^2 + a_i^2 = \epsilon^2 + a_i^2$ to get

$$\mathbb{E}(\hat{a}_1 \hat{a}_2 - a_1 a_2)^2 = (\epsilon^2 + a_1^2)(\epsilon^2 + a_2^2) - a_1^2 a_2^2 = \epsilon^4 + (a_1^2 + a_2^2)\epsilon^2 \leq 2\epsilon^2 + \mathcal{O}(\epsilon^4). \quad (29)$$

Using the same technique for the case of general n yields:

$$\mathbb{E} \left(\prod_i \hat{a}_i - \prod_j a_j \right)^2 = \prod_i (\epsilon^2 + a_i^2) - \prod_j a_j^2 = \epsilon^2 \sum_i \prod_{j \neq i} a_j^2 + \mathcal{O}(\epsilon^4) \leq n\epsilon^2 + \mathcal{O}(\epsilon^4). \quad (30)$$

□

In addition, we review the *Schwarz Inequality* [35] in the context of probability theory.

Lemma 3. Let \hat{a} and \hat{b} be two random variables with means a and b respectively. Then the following inequality holds:

$$\left| \text{Cov}(\hat{a}, \hat{b}) \right| \leq \text{std}(\hat{a}) \text{std}(\hat{b}) \quad (31)$$

where $\text{Cov}(\hat{a}, \hat{b}) = \mathbb{E}(\hat{a} - a)(\hat{b} - b)$.

Proof of Theorem 1. Without loss of generality, assume the fragments considered has been reduced with respect of operator O (c.f. Section 2.1). Recall the circuit cutting formula presented in Eq. (14). Using procedures from shadow tomography (c.f. lemma 1), we seek to estimate each trace-term in the product to η additive error with probability $1 - \gamma$. Our goal is to find the corresponding η and γ such that the total error, upon adding and multiplying, gives an error of ϵ with probability $1 - \delta$.

Let $\mu = \text{tr}(O\rho)$ and $\hat{\mu}$ denote the estimator derived from the divide-and-conquer shadow tomography. Moreover, let $\tau(\mathbf{M}, P)$ be a shorthand for the product of trace terms in Eq. (14) and $\hat{\tau}(\mathbf{M}, P)$ be the corresponding estimator, *i.e.*

$$\hat{\mu} = \sum_{P \in \{I, X, Y, Z\}^{\otimes |\kappa|}} \alpha_P \sum_{\mathbf{M} \in \mathcal{B}^{|E_{\Delta}|}} \hat{\tau}(\mathbf{M}, P) \quad (32)$$

We can bound the variance of $\hat{\mu}$:

$$\text{Var}(\hat{\mu}) = \sum_{P, P'} |\alpha_P|^2 |\alpha_{P'}|^2 \text{Cov} \left(\sum_{\mathbf{M}} \hat{\tau}(\mathbf{M}, P), \sum_{\mathbf{M}'} \hat{\tau}(\mathbf{M}', P') \right) \quad (33)$$

$$\leq \sum_{P, P'} |\alpha_P|^2 |\alpha_{P'}|^2 \sum_{\mathbf{M}, \mathbf{M}'} \text{std}(\hat{\tau}(\mathbf{M}, P)) \text{std}(\hat{\tau}(\mathbf{M}', P')) \quad (34)$$

$$= \left(\sum_{P, \mathbf{M}} |\alpha_P|^2 \text{std}(\hat{\tau}(\mathbf{M}, P)) \right)^2 \quad (35)$$

$$\leq \left(\sum_{\mathbf{M}} \left(\sum_P |\alpha_P|^2 \right) \max_{P', \mathbf{M}'} \{ \text{std}(\hat{\tau}(\mathbf{M}', P')) \} \right)^2 \quad (36)$$

$$= \left(4^{|E_{\Delta}|} \|O\|_{\mathbb{S}}^2 \max_{P, \mathbf{M}} \{ \text{std}(\hat{\tau}(\mathbf{M}, P)) \} \right)^2 \quad (37)$$

where the first inequality is by Schwarz inequality (c.f. Lemma 3), and

$$\|O\|_{\mathbb{S}} = \sqrt{\text{tr}(O^\dagger O) / 2^{N_q}} \quad (38)$$

is the ‘‘Pauli-string’’ norm of O .

Note that, while $\hat{\tau}$ ’s are not independent of each other, terms inside $\hat{\tau}$ are. Thus, by Lemma 2, we can bound the standard deviation of the last term in Eq. (37).

$$\max_{P, \mathbf{M}} \{ \text{std}(\hat{\tau}(\mathbf{M}, P)) \} \leq (|\kappa| + |\Gamma|) \eta + \mathcal{O}(\eta^2) \quad (39)$$

So, the standard deviation of $\hat{\mu}$ is bounded by:

$$\text{std}(\hat{\mu}) = 4^{|E_{\Delta}|} \|O\|_{\mathbb{S}}^2 \sqrt{(|\kappa| + |\Gamma|) \eta + \mathcal{O}(\eta^2)} \quad (40)$$

Note that the upper bound above holds with probability at most $(1 - \gamma)^{|F|} = 1 - |F|\gamma + \mathcal{O}(\gamma^2) = \delta$. Thus, using Lemma 1, we get the sample complexity per fragment by rescaling η and γ to be with respect to ϵ and δ .

$$K_{f_k} = 2 \log \frac{2|F| \cdot 4^{\text{qdeg}(f_k)}}{\delta}, \quad N_{f_k} = \frac{34 \cdot 16^{|E_{\Delta}|} (|\kappa| + |\Gamma|) \|O\|_{\mathbb{S}}^4 4^{\text{deg}(f_k)}}{\epsilon^2} \quad (41)$$

For each fragment, we must build shadows capable of inferring all quantum degrees of freedom, leading to the factor of $4^{\text{qdeg}(f_k)}$ in K_{f_k} for estimating $\text{qdeg}(f_k)$ many expectations. Moreover, the size of the operators acting on fragment f_k is the sum of the size of O on the circuit output of f_k in addition to the quantum degrees of freedom; hence, $4^{\text{deg}(f_k)}$ factor in N_{f_k} accounts for total size of the operator acting on the Choi state of f_k . Upon rearranging, we arrive at the form of Eq. (26). \square

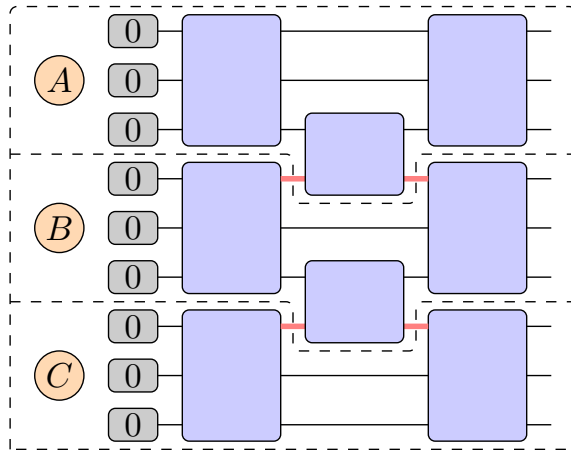


Figure 3: Clustered circuit ansatz with three fragments labeled A, B, and C above. Each purple block represents a Haar-random gate on the corresponding qubits. This figure reproduced from Ref. [24] with the permission of the authors.

Similar to the existing analysis of circuit cutting in the literature, estimating expectations using fragmentation scale exponentially with the number of cuts, which upper bounds $|E_{\Delta}|$ (specifically, $|E_{\Delta}|$ is the number of cuts between the fragments that are “relevant” for computing the expectation value of O). It is also worth noting that the bound presented is pessimistic in the sense that we took an absolute error from Lemma 1 as standard deviation. Thus, we can expect the error to be considerably lower in practice so long as the additive error η and “failure” probability γ are small.

4.2 Numerical Results

Many components involved in Theorem 1 are dependent on the particular circuit that one chooses to run. Hence, we would like to establish some preliminary numerical results that depict the differences between shadow tomography on unfragmented circuits and our proposed divide and conquer method. We implement the algorithm by adapting PennyLane’s circuit cutting and shadow tomography functions [34]. We run our experiments using a clustered-circuit ansatz (c.f. Figure 3) comprised of Haar-random gates. Each circuit was paired with a randomly generated Pauli observable of a chosen size. We examined the scaling behavior of the two methods with respect to the number of samples (denoted by shots), the size of the observable (denoted by $\text{size}(O)$), and the number of fragments (denoted by $|F|$). We repeat each experimental setting 250 times with different randomly-generated circuit-observable pair. The results are displayed in Figure 4.

Advantageous regimes For a fixed circuit, fragmentation significantly improves the estimated expectation when large observables are being estimated. This is evident in each panel in the bottom row of Figure 4. As the weight of an observable O grows, the difference in accuracy between regular shadow tomography ($|F| = 1$) and fragmented shadow tomography increases. Since each fragment is only “responsible” for the part of O that directly affects the qubits in the fragment, circuit cutting divides the observable into smaller parts. Recall that the sample complexity of shadow tomography scales exponentially with respect to the weight of the observable. As the number of fragments increases, the average per-fragment weight of each observable decreases proportionally, which then lowers the sample complexity by an exponential factor. This shrinkage in the size of O on a frag-

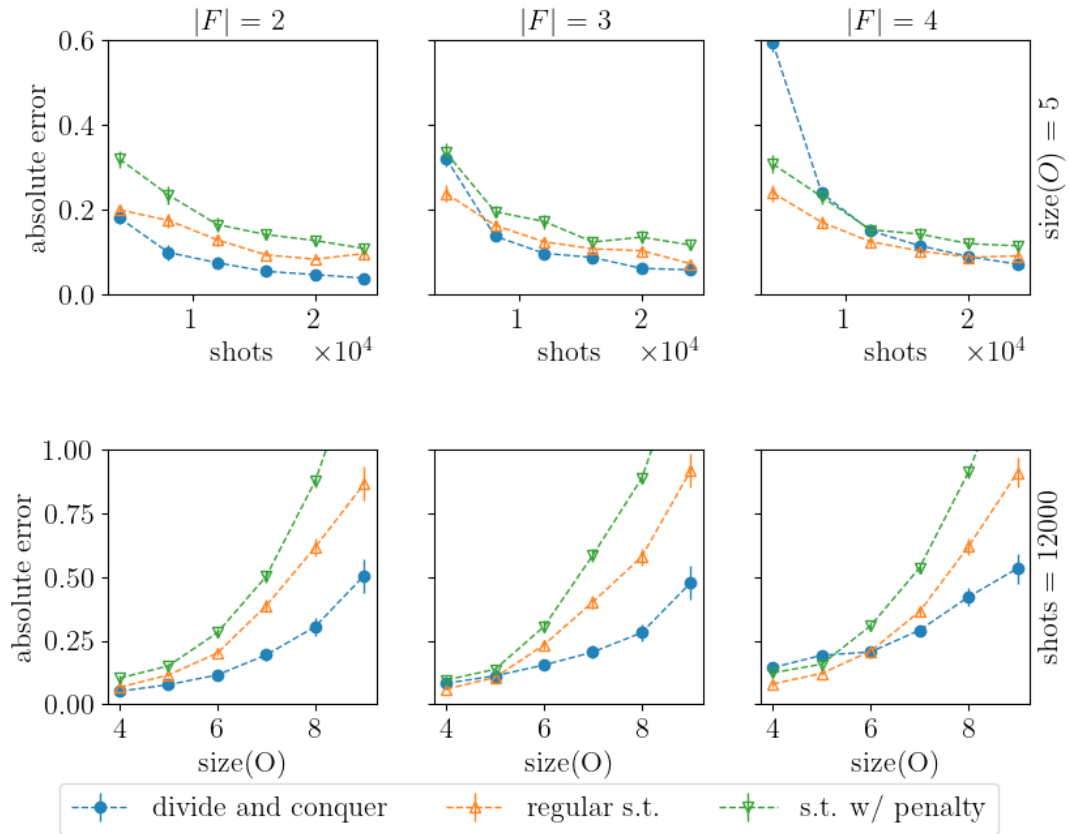


Figure 4: Numerical results comparing estimates obtained from shadow tomography with (blue) and without (orange) fragmentation. The estimate can be penalized (green) if it was an uninformed guess. The lower the absolute error, the closer the estimated expectation is to the true expected value. **(top row)** The absolute error with respect to the number of shots (classical shadows) across different numbers of fragments. **(bottom row)** The absolute error with respect to the size of the randomly generated observable across different numbers of fragments.

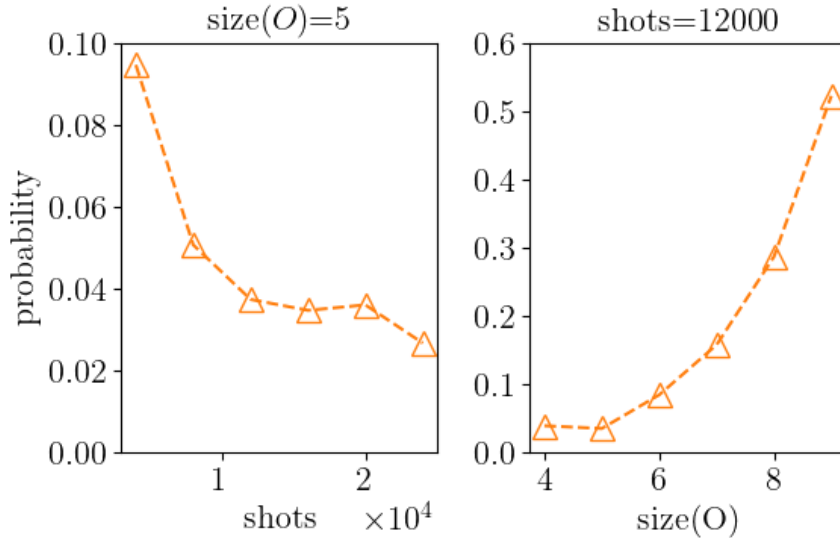


Figure 5: The probability of not observing the Pauli string of interest with respect to **(left)** the number of shots and **(right)** the size of the Pauli string.

ment results in an increasing separation between fragmented and unfragmented shadow tomography.

However, the justification above significantly understates the benefit of fragmentation when estimating expectations of large observables. Recall Section 3.1—if the sequence of the observable being estimated is not present in the ensemble of classical shadows, we return a default value of zero. Meanwhile, for any Pauli observable P and state ρ induced by the circuit ansatz in Figure 3 comprised of only Haar-random unitaries, one should expect that $\mathbb{E}_{(\rho, P) \sim \text{Ansatz}} \text{tr}(P\rho) = 0$, where $\mathbb{E}_{(\rho, P) \sim \text{Ansatz}}$ denotes an average over choices of Haar-random gates defining ρ and fixed-size observables P . Moreover, we can also expect a shrinking variance with $(\rho, P) \sim \text{Ansatz}$ in the limit of large circuit size, which means that the individual terms in this average approach zero as well. Although under regular circumstances, outputting the uniform prior as an a priori estimate is the least-informed guess that one can make, in our numerical experiment, zero is actually a high quality guess!

We can study the empirical probability of such phenomenon occurring, c.f. Figure 5. It turns out that for large observables, the desired Pauli string is only observed roughly half of the times. The number of shots is an influencing factor, too. However, it has much less of an effect compared to the observable weight. Nonetheless, both trends can be explained through the same rationale: the number of shots dedicated to each degree of freedom is too low. To further emphasize this point, we provide a (moderate but arbitrary) penalty for making an uninformed guess for the expectation value of an operator, shown in the green lines in Figure 4. The penalty widens the already existing gap between regular and fragmented shadow tomography, especially when the number of shots is low and the weight of the observable is high. In conclusion, we expect fragmentation to be a beneficial procedure when the observable is large, and particularly so when the quantum resources are scarce.

Limits of fragmentation Though there are circumstances where fragmentation is beneficial, is it necessarily the case that more fragments the merrier? The answer is no! First,

it is evident from the top row of Figure 4 that fragmentation is not advantageous when low number of shots are available. Recall that there is an extra degree of freedom to infer per incident of cut on a fragment. Consequently, the number of samples needed to properly account for the additional uncertainty grows exponentially with the number of incident cuts on a fragment. Thus, when quantum resources are scarce, the drawback of not having enough shots to characterize each fragment well often outweighs the benefit of avoiding having unobserved Pauli strings as described before, resulting in poor estimates.

Given sufficient samples, there also exist regimes in which fragmentation can be harmful. Observe the scaling with respect to fragments on the bottom row of Figure 4. For small observables, increasing the number of fragments inflates the absolute error as well. On the other hand, fragmentation does not take much effect for a size-9 observable. This implies that the rate at which the error increases is lower when many cuts are present. Thus, as discussed before, splitting the circuit for large observables is beneficial. However, for low-weight operators, excessive cutting can introduce undesirable degrees of freedom that need to be inferred.

5 Conclusions

In this paper, we introduced fragmented shadow tomography, a novel divide-and-conquer method for building classical shadows while incorporating circuit cutting procedures. This method combines the benefits of both of its predecessors—efficient computation and storage of quantum states through classical shadows and the ability to be parallelized in independent quantum simulators/devices. We derived a general formula to combine shadow tomography estimates of each fragment. Moreover, we provide the respective sample complexity for each fragment such that the total additive error is bounded to desired precision. Lastly, we numerically demonstrated its advantages over traditional, unfragmented shadow tomography, exceedingly so when large observables are of interest.

We focused on building classical shadows including all components—quantum input, quantum output, and circuit output—of a fragment. This need not be the case. One can also consider partially derandomizing fragmented shadow tomography by building classical shadows only on circuit outputs. That is, for all quantum inputs and outputs, *i.e.* $\mathbf{M} \in \mathcal{B}^{|E_{\Delta}|}$, we can replace randomized Pauli measurements with deterministic initialization/measurement schemes, keeping the randomized procedure only for circuit outputs. Each classical shadow will be a function of M_{f_k} and the respective Choi matrices can be inferred via maximum likelihood procedures (c.f. [24]). The two methods are equivalent in the large sample limit. However, we expect derandomization will bring statistical stability under finite computational resources. Derandomization may also reduce errors, as in Ref. [2].

When examining the numerical results, we see a trade-off between the number of fragments and the size of the observable. For small observables, excessive fragmentation leads to accumulation of error and decrease in number of shots attributed to each fragment. On the other hand, dividing circuits becomes beneficial for large observables that would require excessively many shots of estimate. Thus, we suspect an existence of an optimal number of cut given a quantum circuit and an observable (or a priori knowledge on the size of the observable). As a consequence of this conjecture, predicting the optimal number of fragments subsequently becomes an important open question to further leverage quantum divide-and-conquer algorithms.

Acknowledgments

The authors thank Nathan Killoran and Thomas Bromley for helpful discussions.

M.A.P. thanks Pranav Gokhale for enabling an environment in which this work was possible.

Z.H.S is supported by the U.S. Department of Energy Office of Science National Quantum Information Science Research Center, QNEXT. D.C. was funded by the SULI fellowship at Argonne National Laboratory.

The submitted manuscript has been created by UChicago Argonne, LLC, Operator of Argonne National Laboratory (“Argonne”). Argonne, a U.S. Department of Energy Office of Science laboratory, is operated under Contract No. DE-AC02-06CH11357. The U.S. Government retains for itself, and others acting on its behalf, a paid-up nonexclusive, irrevocable worldwide license in said article to reproduce, prepare derivative works, distribute copies to the public, and perform publicly and display publicly, by or on behalf of the Government. The Department of Energy will provide public access to these results of federally sponsored research in accordance with the DOE Public Access Plan (<http://energy.gov/downloads/doe-public-access-plan>).

Conflict of Interest The authors declare that they have no conflict of interest.

References

- [1] S. Aaronson, “Shadow tomography of quantum states”, *SIAM Journal on Computing* **49**, STOC18–368 (2019).
- [2] H.-Y. Huang, R. Kueng, and J. Preskill, “Predicting many properties of a quantum system from very few measurements”, *Nature Physics* **16**, 1050–1057 (2020).
- [3] A. Elben, S. T. Flammia, H.-Y. Huang, R. Kueng, J. Preskill, B. Vermersch, and P. Zoller, “The randomized measurement toolbox”, *arXiv preprint*, DOI: 10.48550/arXiv.2203.11374 (2022), [arXiv:2203.11374 \[quant-ph\]](https://arxiv.org/abs/2203.11374).
- [4] H.-Y. Huang, “Learning quantum states from their classical shadows”, *Nature Reviews Physics* **4**, 81–81 (2022).
- [5] H.-Y. Huang, R. Kueng, and J. Preskill, “Efficient estimation of pauli observables by derandomization”, *Physical review letters* **127**, 030503 (2021).
- [6] R. Stricker, M. Meth, L. Postler, C. Edmunds, C. Ferrie, R. Blatt, P. Schindler, T. Monz, R. Kueng, and M. Ringbauer, “Experimental single-setting quantum state tomography”, *arXiv preprint* (2022), [arXiv:2206.00019 \[quant-ph\]](https://arxiv.org/abs/2206.00019).
- [7] J. M. Lukens, K. J. Law, and R. S. Bennink, “A bayesian analysis of classical shadows”, *npj Quantum Information* **7**, 1–10 (2021).
- [8] H.-Y. Huang, S. T. Flammia, and J. Preskill, “Foundations for learning from noisy quantum experiments”, *arXiv preprint* (2022), [arXiv:2204.13691 \[quant-ph\]](https://arxiv.org/abs/2204.13691).
- [9] H.-Y. Huang, M. Broughton, J. Cotler, et al., “Quantum advantage in learning from experiments”, *Science* **376**, 1182–1186 (2022).
- [10] S. H. Sack, R. A. Medina, A. A. Michailidis, R. Kueng, and M. Serbyn, “Avoiding barren plateaus using classical shadows”, *PRX Quantum* **3**, 020365 (2022).
- [11] A. Zhao, N. C. Rubin, and A. Miyake, “Fermionic partial tomography via classical shadows”, *Physical Review Letters* **127**, 110504 (2021).

- [12] A. Seif, Z.-P. Cian, S. Zhou, S. Chen, and L. Jiang, “Shadow distillation: quantum error mitigation with classical shadows for near-term quantum processors”, arXiv preprint (2022), [arXiv:2203.07309 \[quant-ph\]](#).
- [13] D. E. Koh and S. Grewal, “Classical shadows with noise”, [Quantum](#) **6**, 776 (2022).
- [14] J. Kunjummen, M. C. Tran, D. Carney, and J. M. Taylor, “Shadow process tomography of quantum channels”, arXiv preprint (2021), [arXiv:2110.03629 \[quant-ph\]](#).
- [15] R. Levy, D. Luo, and B. K. Clark, “Classical Shadows for Quantum Process Tomography on Near-term Quantum Computers”, arXiv preprint (2021), [arXiv:2110.02965 \[quant-ph\]](#).
- [16] A. Warshel and M. Levitt, “Theoretical studies of enzymic reactions: dielectric, electrostatic and steric stabilization of the carbonium ion in the reaction of lysozyme”, [Journal of molecular biology](#) **103**, 227–249 (1976).
- [17] M. S. Gordon, D. G. Fedorov, S. R. Pruitt, and L. V. Slipchenko, “Fragmentation methods: a route to accurate calculations on large systems”, [Chemical reviews](#) **112**, 632–672 (2012).
- [18] W. Li, S. Li, and Y. Jiang, “Generalized energy-based fragmentation approach for computing the ground-state energies and properties of large molecules”, [The Journal of Physical Chemistry A](#) **111**, 2193–2199 (2007).
- [19] H. Li, W. Li, S. Li, and J. Ma, “Fragmentation-based qm/mm simulations: length dependence of chain dynamics and hydrogen bonding of polyethylene oxide and polyethylene in aqueous solutions”, [The Journal of Physical Chemistry B](#) **112**, 7061–7070 (2008).
- [20] T. Peng, A. W. Harrow, M. Ozols, and X. Wu, “Simulating large quantum circuits on a small quantum computer”, [Physical Review Letters](#) **125**, 150504 (2020).
- [21] Z. H. Saleem, T. Tomesh, M. A. Perlin, P. Gokhale, and M. Suchara, “Quantum Divide and Conquer for Combinatorial Optimization and Distributed Computing”, arXiv preprint (2021), [arXiv:2107.07532 \[quant-ph\]](#).
- [22] T. Ayral, F.-M. Le Régent, Z. Saleem, Y. Alexeev, and M. Suchara, “Quantum divide and compute: hardware demonstrations and noisy simulations”, in [2020 IEEE Computer Society Annual Symposium on VLSI \(ISVLSI\)](#) (IEEE, 2020), pp. 138–140.
- [23] T. Ayral, F.-M. L. Régent, Z. Saleem, Y. Alexeev, and M. Suchara, “Quantum divide and compute: exploring the effect of different noise sources”, [SN Computer Science](#) **2**, 1–14 (2021).
- [24] M. A. Perlin, Z. H. Saleem, M. Suchara, and J. C. Osborn, “Quantum circuit cutting with maximum-likelihood tomography”, [npj Quantum Information](#) **7**, 1–8 (2021).
- [25] A. Lowe, M. Medvidović, A. Hayes, L. J. O’Riordan, T. R. Bromley, J. M. Arrazola, and N. Killoran, “Fast quantum circuit cutting with randomized measurements”, arXiv preprint (2022), [arXiv:2207.14734 \[quant-ph\]](#).
- [26] D. Chen, B. Baheri, V. Chaudhary, Q. Guan, N. Xie, and S. Xu, “Approximate quantum circuit reconstruction”, in [2022 IEEE International Conference on Quantum Computing and Engineering \(QCE\)](#) (IEEE Computer Society, 2022), pp. 509–515.
- [27] C. Piveteau and D. Sutter, “Circuit knitting with classical communication”, arXiv preprint (2022), [arXiv:2205.00016 \[quant-ph\]](#).

- [28] J. M. Renes, R. Blume-Kohout, A. J. Scott, and C. M. Caves, “Symmetric informationally complete quantum measurements”, *Journal of Mathematical Physics* **45**, 2171–2180 (2004).
- [29] J. de Pillis, “Linear transformations which preserve hermitian and positive semidefinite operators”, *Pacific Journal of Mathematics* **23**, 129–137 (1967).
- [30] A. Jamiolkowski, “Linear transformations which preserve trace and positive semidefiniteness of operators”, *Reports on Mathematical Physics* **3**, 275–278 (1972).
- [31] M.-D. Choi, “Completely positive linear maps on complex matrices”, *Linear algebra and its applications* **10**, 285–290 (1975).
- [32] W. Tang, T. Tomesh, M. Suchara, J. Larson, and M. Martonosi, “CutQC: using small quantum computers for large quantum circuit evaluations”, in *Proceedings of the 26th acm international conference on architectural support for programming languages and operating systems* (2021), pp. 473–486.
- [33] R. O’Donnell and J. Wright, “Efficient quantum tomography”, in *Proceedings of the forty-eighth annual acm symposium on theory of computing* (2016), pp. 899–912.
- [34] V. Bergholm, J. Izaac, M. Schuld, C. Gogolin, M. S. Alam, S. Ahmed, J. M. Arrazola, C. Blank, A. Delgado, S. Jahangiri, et al., “PennyLane: automatic differentiation of hybrid quantum-classical computations”, arXiv preprint (2018), [arXiv:1811.04968 \[quant-ph\]](https://arxiv.org/abs/1811.04968).
- [35] E. Çinlar, *Probability and Stochastics*, Vol. 261 (Springer, 2011).